Contents lists available at ScienceDirect

Comptes Rendus Mecanique

Mechanics of granular and polycrystalline solids

A DEM analysis of step-path failure in jointed rock slopes

Luc Scholtès [a,*], Frédéric V. Donzé [b]

[a] Université de Lorraine/CNRS/CREGU, UMR 7359 GeoRessources, BP 40, 54501 Vandœuvre-lès-Nancy, France
[b] Université Joseph Fourier-Grenoble-1/Grenoble INP/CNRS, UMR 5521 3SR, 38041 Grenoble cedex 9, France

A R T I C L E   I N F O

A B S T R A C T

A numerical analysis of step-path failure mechanisms in rock slopes is provided based upon simulations performed using a discrete element method specifically enhanced for the modeling of jointed rock masses. Fracturing of the intact rock as well as yielding within discontinuities can be simulated to determine the failure surface without any a priori assumption on its location. For both coplanar and non-coplanar sets of discontinuities, failure is the result of the propagation of tensile microcracks that develop in the rock bridges from the tips of pre-existing discontinuity planes in a way similar to wing cracks extensions that can eventually coalesce to form extended step-path failure surfaces. Sensitivity analyses are performed to better understand the critical mechanisms that lead to slope failure and to discriminate between the respective roles played by intact rock and planes of weakness at the onset of failure. For a randomly distributed set of joints that share the same preferential orientation, failure is shown to be dependent on the frictional strength mobilized on the joint surfaces. The results confirm the critical need for a comprehensive and extensive characterization of both mechanical and geometrical properties of discontinuities when assessing the stability of a rock mass.

1. Introduction

Numerical modeling is now widely used in civil and mining engineering to assess stability of rock slopes for safety and economic purposes. However, conventional continuum or classical discontinuum methods experience some limitations to realistically simulate the progressive failure of jointed rock slopes [1,2]. The ability to describe kinematic release through fracturing is a key issue in rock slope stability analysis that cannot be addressed by conventional numerical models. Indeed, assumptions of fully persistent discontinuity sets are only valid in cases where small rock volumes are concerned in the failure process. Moreover, translational rock slope failures generally involve combined failure mechanisms where a complex interaction occurs between pre-existing discontinuities and intact rock bridges whose respective strengths are not necessarily mobilized simultaneously [3–7]. It is therefore critical to consider not only sliding and opening along pre-existing discontinuities but also the possibility of rock bridge failure when assessing the stability of a rock mass.

In slope stability analysis, the objective is to determine the critical factors that control failure to evaluate and anticipate post-failure consequences. In addition to the rock mass strength, these critical factors include the persistence and spacing of the discontinuities as well as their hydro-mechanical properties (cohesion, frictional strength, stiffness, dilation, conductivity, etc.). For several years now, a subsequent effort has been made toward the development of numerical methods able to

---

* Corresponding author. Tel.: +33 383 596 371.
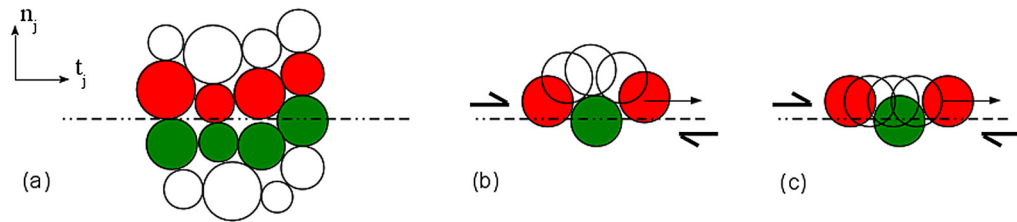 *E-mail address:* luc.scholtes@univ-lorraine.fr (L. Scholtès).

Fig. 1. (Color online.) Illustration of the plane contact logic. (a) A plane segment representing a discontinuity (or joint) overlaid on the discrete elements set. (b) Displacements induced by shearing along a discontinuity plane using the classic contact logic. (c) Displacements induced by shearing along a discontinuity plane using the modified contact logic: the normal and tangential directions to the contact are defined by the joint orientation (n_j, t_j) and not by the particles' contact geometry.

reproduce the progressive failure mechanisms occurring in jointed rock slopes [1,8–10], but it is only recently that complete formulations capable of describing crack initiation and propagation in 3D have been proposed [11–13].

The work presented here is devoted to the application of one of these recently developed numerical approaches to the study of rock slope stability, emphasizing cases where failure occurs through the combination of shearing along discontinuity surfaces and fracturing of the intact rock matrix, the so-called "step-path" failure mode. The formulation of the method is an offspring from the discrete element method which provides the capability of simulating brittle fracture propagation through breakage of the cohesive bonds defined between the particles making up the intact part of the material. As an upgrade to previous attempts made to simulate rock slopes failure using a particulate mechanics approach [8], the method has been recently enhanced with a dedicated feature that provides an efficient and constitutive manner to describe pre-existing fractures and which has proven to capture accurately progressive failure mechanisms in both intact and jointed rock [12,14,15].

In order to identify the parameters likely to play a decisive role in the development of step-path failure surfaces and subsequent translational slope movements, several rock slope configurations involving different joint set patterns were simulated. After a brief description of the model formulation, referenced case studies involving a unique rock bridge are examined in the framework of fracture mechanics with reference to previous works [5]. A sensibility analysis is then proposed in order to emphasize the effects the geometry and the mechanical properties of a given pre-existing joint set can have on slope stability. Finally, the failure mechanisms of a rock slope associated with a more realistic fracture network configuration involving several joint sets are discussed on the basis of the model's predictions.

2. Formulation of the method

The proposed method is implemented into the YADE Open DEM platform [16–18], an extendable open-source framework for numerical modeling based on the discrete element method (DEM). As initially proposed by Cundall and Strack [19], the simulated medium is represented as an assemblage of rigid particles (also called discrete elements) in interaction with each other through force-displacement laws that can be adapted in accordance to the material to be modeled. In the present work, particles are bonded together following a linear elastic–plastic law which has proven to be well adapted to simulate cohesive-frictional materials [14]. As for classical DEM, the algorithm involves two steps. First, according to the loading imposed on the numerical assembly, forces are computed between discrete elements (DE) in interaction with each other. Then, Newton's second law is used to determine, for each DE, the resulting acceleration, which is then time integrated to find the new element positions. This process is thus repeated iteratively according to the prescribed loading path. Because of its formulation, the method can simulate highly nonlinear behaviors characteristic of brittle materials as a result of local bond breakage in both tensile and shear failure modes. In order to better simulate rock-like behaviors, YADE's formulation has been recently upgraded with a specific feature dedicated to render material texture [14]. Specifically, it has been shown that, by controlling the density of contacts per particle, the degree of interlocking of the DE constituting the numerical medium could be adjusted to mimic the microstructure of the material to model. By doing so, the simulated behavior can be accurately adjusted to reproduce the characteristic features of brittle rock, i.e. a high value of the tensile strength to compressive strength ratio and a non-linear failure envelope, which is not possible with classical DEM formulation (see [14] for details).

In addition, the code has been enhanced to take explicitly into account pre-existing discontinuities (or joints) into its formulation [12,15]. Inspired from the smooth-joint contact logic developed by Cundall and co-authors for the development of the Synthetic Rock Mass [20], discontinuities are considered as planar surfaces which can be overlaid on the discrete element set. The interaction forces between DE located on each side of a discontinuity surface can thus be identified and reoriented depending on the normal and tangential directions of the plane as illustrated in Fig. 1.

Using this specifically adapted contact logic, the structural effect induced by discontinuities on the fabric of the medium can be explicitly accounted for, ensuring furthermore a constitutive behavior of the simulated joint surface as demonstrated in [12]. Indeed, contrary to the classic contact logic, the enhanced scheme enables to simulate a behavior that is not dependent on the resolution or roughness of the joint surface which emerges from the spherical shape of the DE. The interface behavior is implemented according to the Mohr–Coulomb theory. The cohesion C, tensile strength T and friction
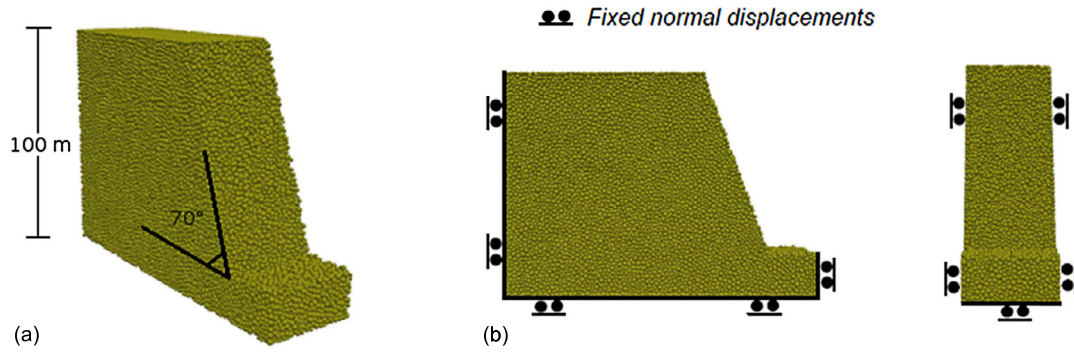
Fig. 2. (Color online.) 3D slope model used in this study. (a) Overall view. (b) Boundary conditions, side and front views.

angle Φ of the joint surface as well as its normal and shear stiffnesses, K_n and K_s, are thus parameters that can be adequately set depending on site or laboratory characterizations. In addition, the opening of the joint with sliding can be taken into account for a more representative description of rock joints behavior as observed in [21]. The details of the numerical implementation are given in [12] and are thus not repeated here.

Finally, for the purpose of the present study, the DEM algorithm was modified so that contact detection between particles is cut off after the first time step of the computation. This feature, which makes the method run in a way similar to a lattice method [22–24], increases computational efficiency as compared to a classic DEM without compromising the integrity of the results as long as the displacements are small compared to the DE size. The study therefore focuses on the onset of failure rather than on the post-failure run-out phase.

3. Simulations description

The proposed method can handle 3D configurations. However, in order to present its capabilities in a clear and comprehensive way, only cross-sectional slices of a slope were studied here (Fig. 2(a)). The slope model consists of a 100 m high slope with a slope face angle of 70°. A set of 75,000 DE were packed into the corresponding closed volume using a dynamic growth technique:

- first, a cloud of non-contacting DE is randomly distributed inside the volume with a uniform size distribution chosen here so as the ratio between the maximum and the minimum radius R_{max}/R_{min} is equal to 2, avoiding therefore the behavioral bias associated with regular packing;
- second, without applying gravity, the size of the DE is progressively increased (in a uniform manner for all DE) until the packing reaches an equilibrium state defined by a stabilization of its porosity over time. The final porosity n of the packing can be adjusted depending on the friction defined between the DE during growth, denser packing being obtained for small values of the friction angle. In the present case, a friction angle of 1° was chosen in order to generate a dense packing with a final porosity $n \approx 0.4$.

Once the packing was generated, boundary conditions were set by preventing the movements of the DE making up the boundaries along the direction perpendicular to the model surface (Fig. 2(b)). All other DE could move in all directions. One has to note here that the model's formulation is size independent so that the behavior of the same volume filled with a different number of DE would present a similar behavior as it has been verified for numerical simulations of laboratory tests in previous studies [25]. The size of the DE (and therefore their number) was chosen here to ensure a sufficient discretization of the interspace between fractures for every tested case. The same packing was used in all the following studies. The model's geometry having been fixed, the loading path had to be defined. In our simulations, gravity was applied to the model before every simulation in order to generate an in-situ stress. The DE density ρ_{DE} was set such that the gravity induced vertical stress σ_v at the bottom boundary of the model corresponds to the one expected for a 100 m high slope consisting of a rock with a density ρ equal to 2500 kg/m³ ($\sigma_v \approx 2.5$ MPa).

The mechanical properties of the rock matrix were chosen here to ensure that the simulated behavior is representative of a brittle rock. A preliminary calibration procedure was run in order to reproduce the behavior of the Fontainebleau sandstone studied by Sulem and Ouffroukh [26] (the calibration procedure is presented in details in [14]). The properties of the medium are summarized in Table 1 and the simulated behavior depicted in Fig. 3. Because of the model formulation and a convenient choice of parameters (Table 2), the non-linearity of the failure envelope as well as a ratio of 10 between the tensile strength and the compressive strength can be simulated. These latter characteristics, which are fundamental to ensure that the model behaves as a brittle material, are set by controlling the degree of interlocking of the particle constituting the medium as it has been discussed in [14]. The degree of interlocking is directly proportional to the number of bonds (or contacts) defined for each particle N which was set equal to 10 here.

Table 1
Macroproperties of the rock matrix.

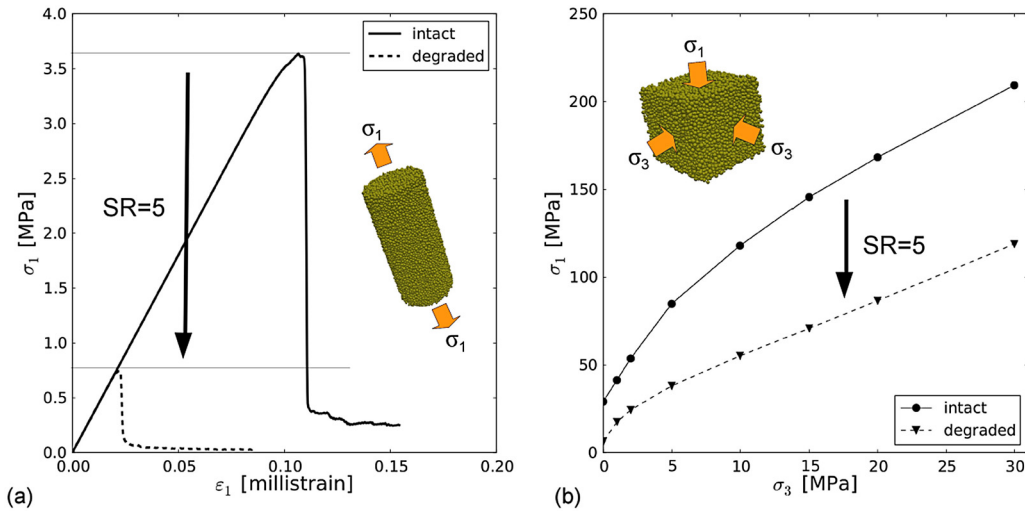| Density ρ (kg/m^3)	Young's modulus E (GPa)	Poisson's ratio υ (−)	Tensile strength UTS (MPa)	Compressive strength UCS (MPa)
2500	45	0.25	3.5	35

Fig. 3. (Color online.) (a) Stress–strain curves obtained from direct tensile test simulations performed on the rock matrix before, and after strength reduction (SR) was operated on its strength properties (see Section 3 for details of the SR method). (b) Predicted failure envelopes for the rock matrix.

Table 2
Microproperties used for the rock matrix (D is the harmonic mean of the interacting DE diameters).

Particle density ρ_{DE} (kg/m^3)	Number of bonds/DE N (−)	Normal stiffness $k_{m,n}/D$ (GPa)	Stiffness ratio $k_{m,s}/k_{m,n}$ (−)	Tensile strength t_m (MPa)	Cohesion c_m (MPa)	Friction angle ϕ_m (°)
4100	10	50	0.3	4.5	45	18

Table 3
Macroproperties of the rock joints.

Normal stiffness K_n (GPa m)	Shear stiffness K_s (GPa m)	Friction angle Φ (°)	Tensile strength T (MPa)	Cohesion C (MPa)	Dilation angle Ψ (°)
4.5	2	30	0	0	0

Table 4
Microproperties used for the rock joints (D is the harmonic mean of the interacting DE diameters).

Normal stiffness $k_{j,n}/D$ (GPa)	Stiffness ratio $k_{j,s}/k_{j,n}$ (−)	Friction angle ϕ_j (°)	Tensile strength t_j (MPa)	Cohesion c_j (MPa)	Dilation angle ψ_j (°)
5	0.1	30	0	0	0

The microproperties of the interaction that make-up the joint planes were calibrated to simulate non-cohesive joint surfaces ($C = 0$, $T = 0$), with a friction angle Φ equal to 30° and a dilation angle Ψ of 0° (Tables 3 and 4). As a first approximation, the stiffness was fixed to be 10 times smaller for the interactions located across the joint planes than for the ones inside the rock matrix. As presented in Fig. 4(a), the elastic-perfectly plastic behavior of the simulated joint surface under direct shear is representative of a typically smooth surface and does not exhibit the softening behavior commonly observed for natural rock joints with rough surfaces. Providing a simplified smooth joint behavior, the approach ensures nonetheless that the behavior is identical whatever the size and orientation of the discontinuity planes, which is a significant improvement over classical contact formulation [8,12,27].

In cases failure did not occur as a result of the prescribed structural and mechanical conditions (due to the presence of rock bridges for instance), a strength reduction (SR) method was applied in order to lead the slope model to failure. As-suming that failure often occurs in nature due to progressive weakening of the rock bridges located in-between pre-existing discontinuities (due to hydro-mechanical couplings, freeze-thaw cycles, chemical weathering, ...), the strength of the in-
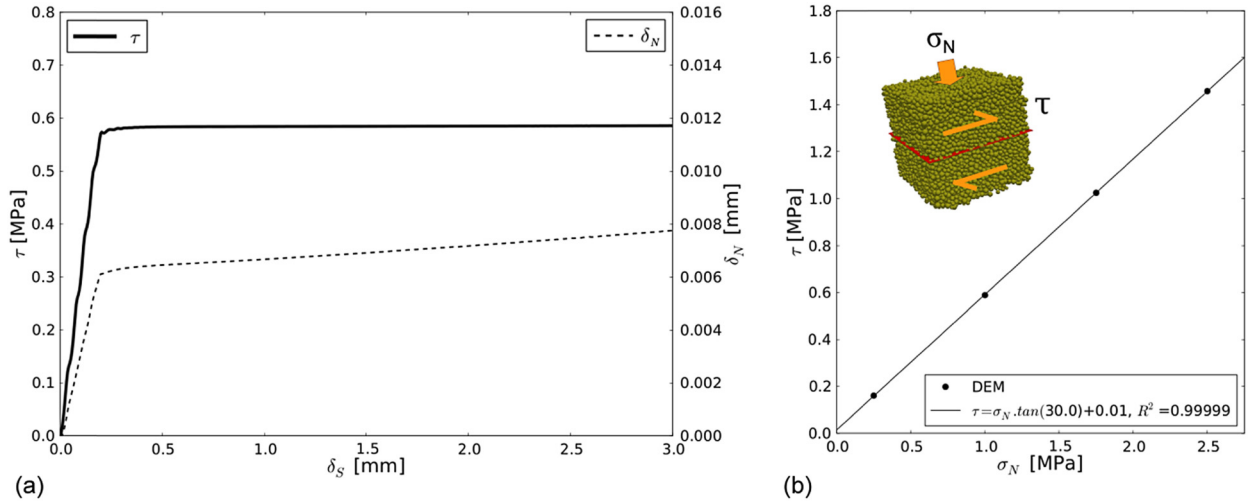
Fig. 4. (Color online.) (a) Stress–strain curves obtained from direct shear test simulations performed on the calibrated model under a constant normal load σ_n equal to 1 MPa: τ is the shear stress and δ_n and δ_s are the normal and the shear displacement of the joint respectively. (b) Predicted failure envelopes for the rock joint.
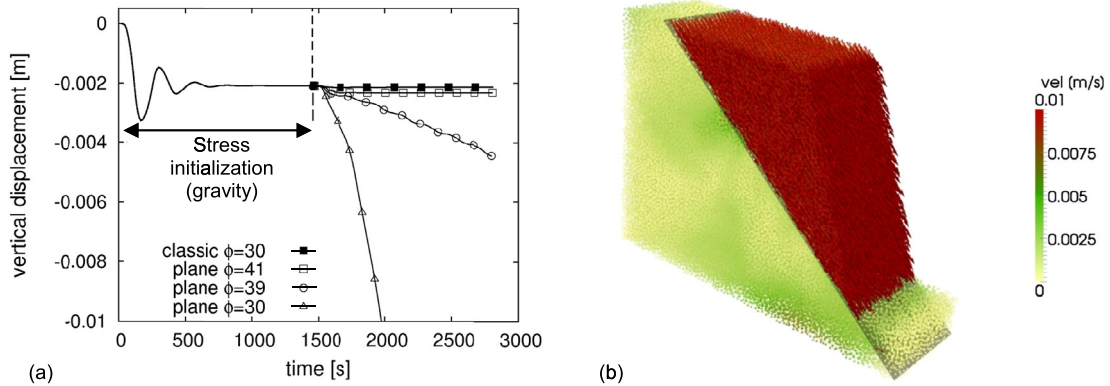

Fig. 5. (Color online.) (a) Evolution of the slope crest displacement as a function of the simulation time for different contact properties of the joint surface (classic and plane contact logic). (b) Velocity field obtained when the friction angle Φ was set to 30° using the plane contact logic.

terparticle bonds making up the intact part of the medium was progressively decreased throughout the simulation (tensile strength t_m and cohesion c_m were reduced by the same amount). The SR factor α, defined as the ratio between the initial strength and the updated assigned strength $\alpha = t_m^{(0)}/t_m^{(t)}$, was thus iteratively increased until the slope deviated from a stable configuration. The stability of the slope was assessed by checking that the velocity v of the DE belonging to the crest of the slope was smaller than a predefined value ($v_0 = 1$ mm/s here). One can note from Fig. 3 that the SR induced at the macroscopic scale is appreciatively proportional to the one assigned at the interparticle scale ($\alpha = t_m^{(0)}/t_m^{(t)} \approx UTS^{(0)}/UTS^{(t)}$) and could thus be of interest if back analyses were used for assessing the potential of a real slope toward failure.

4. Results

4.1. Persistent plane

A configuration involving the predefined slope model cut by a persistent joint dipping at 40° toward the slope face was first studied (Fig. 5). Once stress initialization is achieved and the slope is stable ($v \ll 1$ mm/s), joint surfaces are assigned their predefined mechanical properties. In order to demonstrate the model capability, the simulation was run under different assumptions:

– using the "classic" contact logic with a friction angle Φ supposedly favorable to failure ($\Phi = 30°$);
– using the plane contact logic for several values of the joint friction angle Φ (30°, 39° and 41° respectively).
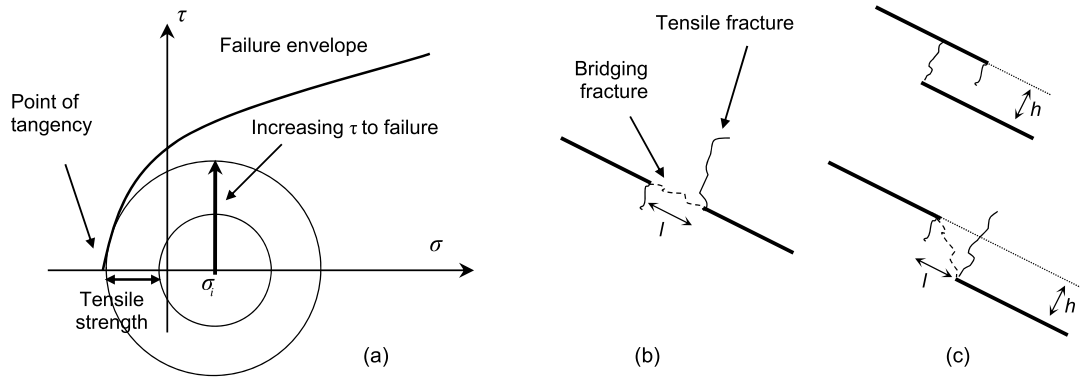
Fig. 6. (a) Mohr's circle – Failure at low stress level σ_i. (b) In plane failure of rock bridge. (c) Out of plane failure of rock bridge: overhanging case ($l < 0$) and non-overhanging case ($l > 0$); modified after [5].

The evolution of the crest displacement as a function of the simulation time is plotted in Fig. 5(a) for each tested case. The velocity field at the end of the simulation (after 2800 s) is presented in Fig. 5(b) for a case where failure occurred (plane contact logic, $\Phi = 30°$).

It can be inferred from the results that, contrary to the classic contact logic, the plane contact logic overrides the intrinsic problem associated with the DE shape by making the model independent of the roughness of the joint surface and thus, independent of its discretization. Indeed, the enhanced contact logic allows controlling the joint properties with a simulated behavior in accordance with the limit equilibrium theory (stable for $\Phi >$ dip angle, and unstable for $\Phi <$ dip angle).

4.2. Non-persistent plane with an intact rock bridge

In order to assess the validity of the model in terms of fracture propagation, two configurations involving respectively "in plane" and "out of plane" potential failure surfaces were studied, sprung from the work of Einstein and co-authors [5]. The methodology was thus applied to rock slopes in which an intact rock bridge separates two respectively coplanar ("in-plane") or non-coplanar ("out-of-plane") discontinuity planes (Figs. 6 and 7). As for the previous case study, the discontinuity planes dipped at 40° inside the slope and the joint friction angle Φ was set to 30° in order to favor failure.

According to fracture mechanics theory, at low stress levels, failure mainly occurs through tensile fracturing (mode-I rupture) that develops at high angles to the direction of shear displacement (Fig. 6(a)). This led Einstein and co-authors [5] to propose that, during an "in plane" failure (Fig. 6(b)), tensile fractures would then first develop in the rock bridge. Then, depending on both the shear strength and the length l of the rock bridge, a bridging fracture would eventually propagate into the direction of sliding (mode-II rupture). In an "out of plane" failure, two scenarios have to be considered depending on the in plane length l of the rock bridge (Fig. 6(c)). On one hand, if the two discontinuity planes are overhanging with respect to each other ($l < 0$), a continuous tensile crack would directly bridge the two planes and trigger sliding. On the other hand, if the two discontinuity planes are now shifted along the direction of sliding ($l > 0$), bridging would eventually occur depending on both the shear strength and the length l of the rock bridge, as for the in plane case.

Model's predictions are presented in Fig. 7 for both in plane and out of plane configurations. The simulations agree preferentially well with the scenarios discussed previously. Moreover, due to the high ratio between the interparticle tensile and shear strengths chosen here (see Table 2), and to the relatively low stress level in the slope model compared to its intrinsic shear strength (Fig. 3), the fracturing actually occurred through interparticle tensile rupture only, in agreement with the theory. In every case, macro-fractures resulted from the coalescence of microcracks developing from the tips of the discontinuity planes in the manner of wing crack extensions [28].

In the out of plane configurations (Figs. 7(a) and 7(b)), fracturing extended upward so as to eventually reach the upper discontinuity plane. Bridging possibly occurred depending on the relative positions of the pre-existing fractures along the sliding direction. When the junction was made (Fig. 7(a)), the entire upper part of the slope destabilized and slid along the surface formed by the two pre-existing joint planes. When bridging did not occur (Fig. 7(b)), fracturing extended towards the slope face, leading to the detachment of a first distinct block that slid along the discontinuity plane. Additional strength degradation was then needed to destabilize the slope crest via the appearance of a tensile fracture developing downward, from the top of the slope to the newly created free surface. A second upper hanging block would then eventually collapse in a toppling manner, rotating around its base.

In the in-plane configuration (Fig. 7(c)), the mechanism was similar to the out of plane case with no overhanging between the two pre-existing discontinuities (Fig. 7(b)). For the tested case, bridging did not occur between the pre-existing joint planes due to the bridge geometrical (l) and mechanical properties predefined here. However, as for case (b), a process zone developed in the region of shearing as a result of tensile fracturing. Configurations with different rock bridge lengths were tested to see whether bridging could be simulated or not. Bridging was possible for small bridge lengths where it developed through the coalescence of "en echelon" cracks resulting from tensile ruptures inclined towards the direction of
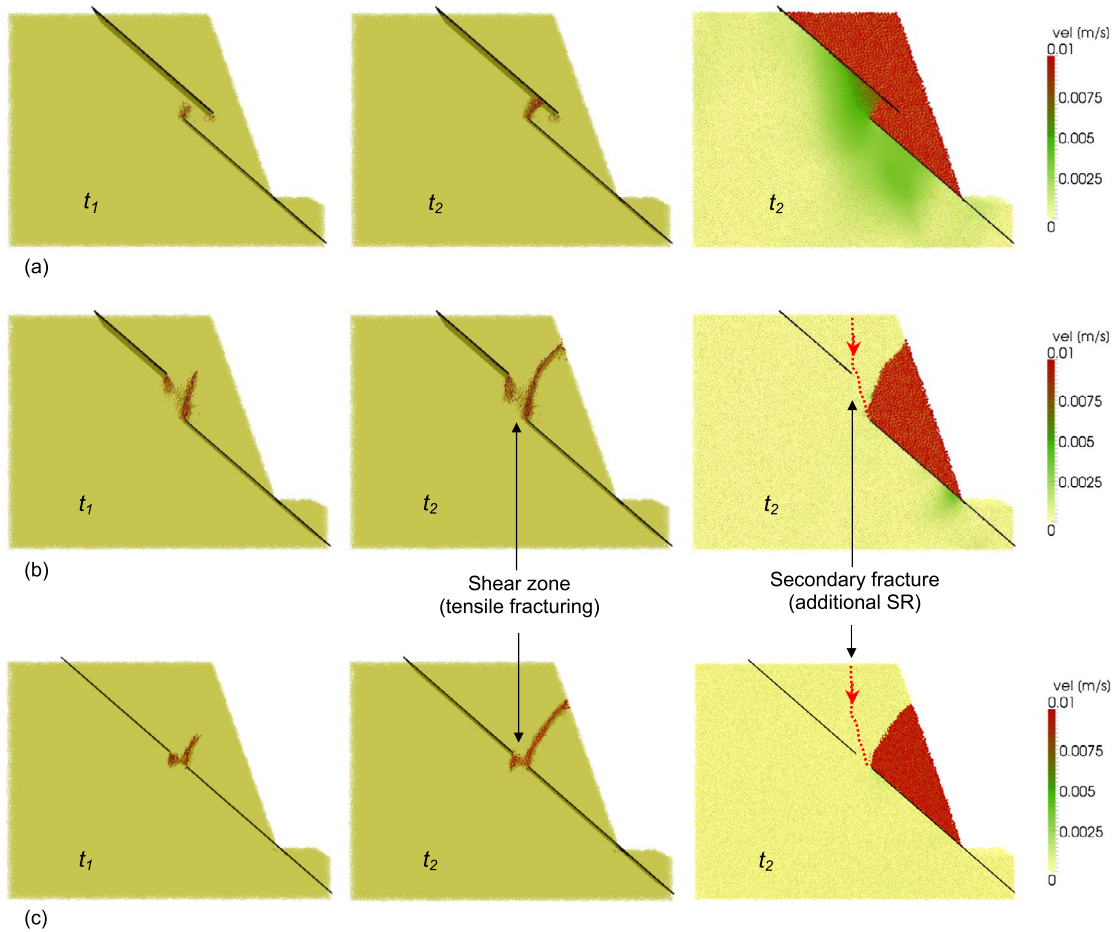
Fig. 7. (Color online.) Fracturing pattern and corresponding final velocity field induced by strength degradation as a function of simulation time t_i $(t_2 > t_1)$ for different rock bridge configurations: (a) out-of-plane case with overhanging joint planes $(l < 0)$, (b) out of plane case with non-overhanging joint planes $(l > 0)$ and (c) in plane case $(l > 0)$.

shearing. This latter result is in accordance with observations made from experiments stating that macro-scale shear failure in brittle rock results from the coalescence of tension induced cracks [29], and emphasizes the importance of tensile fracturing in the development of shear zones at low normal stresses. One has to note however, that in reality, depending on the rock type and on the considered scale, rock bridges fracturing may be complicated by the presence of cross joints which can modify this tendency. This latter issue is of importance and would need further dedicated studies.

4.3. Randomly distributed joint sets

The ability of the model to deal with failure propagation being validated for relatively basic configurations, the following results present case studies where pre-existing joints are not restrained to major failure surfaces, but rather are randomly distributed inside the rock slope. A parametric study is provided so as to demonstrate the potential interest of the methodology for sensitivity analysis of rock slope stability.

4.3.1. Effect of joint properties

In order to emphasize the role of joint set properties on stability, a slope model was built with a randomly distributed joint set dipping 40° towards the slope face (Fig. 8). Here again, gravity was first applied and strength reduction was then iteratively operated until the slope crest destabilized. Model predictions obtained for the reference case conducted with a joint friction angle Φ equal to 30° and a ratio of 10 between the matrix stiffness and the joint stiffness is presented in Fig. 8. Without any a priori assumptions on the location and shape of the potential failure surface, failure occurred in an "en échelon" manner as a result of the progressive fracturing of rock bridges developing within the zones where the material strength was insufficient to support the load. The final failure surface thus consists in a combination of joint sliding surfaces and coalesced tensile fractures typical of step path failure mechanisms.
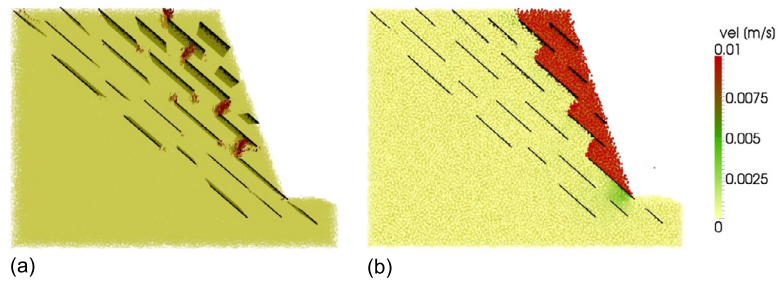
Fig. 8. (Color online.) (a) Fracture pattern at failure and (b) corresponding velocity field for a joint set dipping 40° into the slope model (reference case 1).

Table 5
Sensitivity analysis for a randomly distributed joint set dipping at 40°.

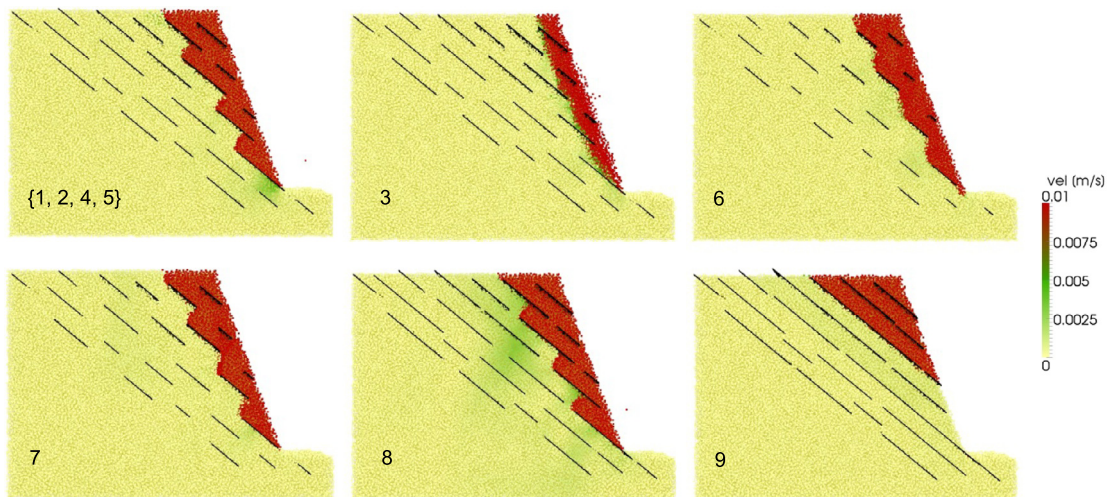| Case	Stiffness ratio – Friction angle – Persistence $K^{(t)}/K^{(0)} - \Phi - L^{(t)}/L^{(0)}$	SR factor at failure $\alpha = UTS^{(0)}/UT^{(t)}$	Collapsing volume (m^3)
1 – reference	1 – 30 – 1	7.5	28,572
2 – friction	1 – 15 – 1	4.2	28,398
3 – friction	1 – 45 – 1	100	11,805
4 – stiffness	0.1 – 30 – 1	5.6	28,130
5 – stiffness	10 – 30 – 1	10	28,760
6 – persistence	1 – 30 – 0.5	32	22,420
7 – persistence	1 – 30 – 0.75	10	26,740
8 – persistence	1 – 30 – 1.25	5.6	26,564
9 – persistence	1 – 30 – 1.5	1	25,332

Fig. 9. (Color online.) Velocity field computed by the model at failure for nine different joint set properties. The parameters of each case study are presented in Table 5.

The simulation was then run varying respectively the mechanical properties (stiffness, friction angle) and the persistence of the discontinuities making up the joint set. Joint persistence was varied by keeping the positions of the barycenter of the pre-existing fractures and by modifying their lengths according to the reference case (case 1), the ratio between the tested joint length $L^{(t)}$ and the reference joint length $L^{(0)}$ being the controlling factor. Table 5 summarizes the parametric study and presents the respective value of the SR factor α needed to trigger failure, as well as the final destabilized volume. The velocity fields predicted by the model at failure are presented in Fig. 9.

Several conclusions can be drawn from the analysis:

– If joint stiffness does not influence the location of the failure surface (cases 1, 4 and 5), it certainly influences the strength of the slopes. Failure occurs for higher matrix strength values (or smaller SR factor) when joint stiffness is smaller. Indeed, larger relative displacements along the joint surface produce a greater concentration of stress at the tips of the discontinuities. Wing cracks then propagate more easily into the rock matrix.
– Joint friction also influences the strength of the slope (cases 1, 2, 3). First, when sliding is possible along the discontinuity planes ($\Phi <$ dip angle; cases 1 and 2), failure occurs for higher matrix strength values when the joint friction
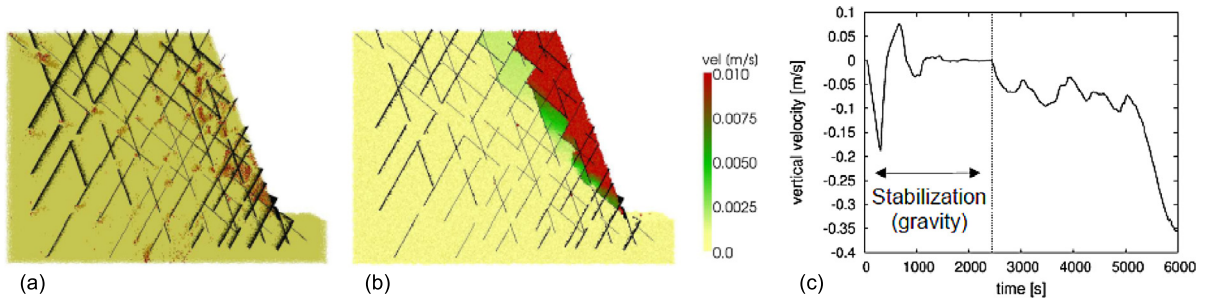
Fig. 10. (Color online.) (a) Cracks pattern, (b) velocity field and (c) history of crest velocity at failure for a simulation performed on a slope with a combination of three joint sets dipping respectively 40°, 70° toward the slope face and 60° backward.

angle is smaller. Certainly, the extra load that cannot be supported by the joint is transferred to the rock matrix which then fails more easily. On the contrary, conservative frictional properties ($\Phi >$ dip angle; case 3) make the slope fail as if it was homogeneous with the development of a superficial circular failure surface which is usually observed in a weak rock or sandy slopes. In this latter case, failure is never reached along the discontinuity planes and stress does not concentrate at the discontinuity tips. Pre-existing fractures are no longer weaknesses in the rock mass and the slope fails as a result of the matrix failure.

These results show how the strength of the slope is distributed between the rock bridges and the joint surfaces depending on their respective strength. It is obvious that the weakest component drives the overall failure. Nonetheless, for a potentially unstable rock mass with a given rock matrix strength, the likelihood of failure is directly dependent on the strength that can be mobilized on the joint surfaces (SR varies from 10 to 4.2 depending on the joint properties).

Besides, joint persistence also has a great influence on slope stability, as the rock mass strength is inversely proportional to the surface occupied by the joints along the potential failure surface. For instance, at least in the tested cases where favorable joint properties where used ($\Phi <$ dip angle) failure occurred for higher values of the matrix strength when the joint surface was increased (cases 6, 7, 8 and 9). This latter result tends to confirm the classical force-balance limit equilibrium solutions for planar-type failures, where the overall shear strength of the slope is inversely proportional to the joint surface, with, however, the ability for the model to deal with non-aligned joint planes.

To sum up, stress concentration in the rock bridges is a function of the strength (or friction) mobilized on the joint surfaces, i.e., larger and weaker joint surfaces induce more deformations along the discontinuities and thus produce higher shear stresses in the rock bridges. Failure is directly constrained by the distribution of strength between the rock matrix and the discontinuities depending on their respective mechanical and geometrical properties.

Although resulting from a particular joint set configuration, the results presented here can be easily extended to more general cases with specific discrete fracture network (DFN) and demonstrate the potential capabilities of the method to determine the parameters most significantly affecting rock mass strength when in situ geological and mechanical data cannot be precisely assessed.

4.3.2. Combined joint sets

In order to complete a simulation of a more realistic rock slope, a model was generated containing a combination of 3 joint sets dipping respectively 40°, 70° toward the slope face and 60° backward (Fig. 10). In addition to the fracturing pattern and the velocity field at failure, the history of the crest velocity is plotted so as to show the timeframe of the simulation.

Contrary to the previous cases with non-persistent joint sets, failure occurred here right after the stabilization of the slope under gravity without any strength reduction applied to the rock matrix. Failure was thus induced as a direct consequence of the joint network configuration. As a first approximation, this result appears consistent with common field observations and classical rock mass strength estimation theory stating that the overall strength of a rock mass decreases with the increase of the fracture density [30]. Interestingly, although the fracture network involved a combination of non-persistent joint sets, blocky structures could be identified in the vicinity of the slope area where failure occurred (Fig. 11(a)). Nonetheless, in the tested case, failure occurred as a consequence of both block movements and intact rock fracturing as demonstrated by simulations performed for higher values of the intact strength for which the slope did not fail. As a consequence of the joint sets configuration, slope movements were a combination of sub-vertical and sub-horizontal sliding preferentially oriented along the 70° and 40° dip angle joint sets. These movements were found to be critically enhanced by flexural toppling mechanisms induced by the joint set dipping 60° toward the rear of the slope. For instance, as seen on the fracturing pattern, microcracking, even though concentrated near the toe of the slope, developed at all depths as a result of large overall displacements. These deeply seated displacements (Fig. 11(b)), characteristics of toppling mechanisms, appeared right after the stabilization phase, mostly induced by the 60° backward dipping joint set as confirmed by additional simulations run for slope models incorporating each of the respective joint sets. In this case study, the 60° dip angle joint set was the driving component for promoting failure.
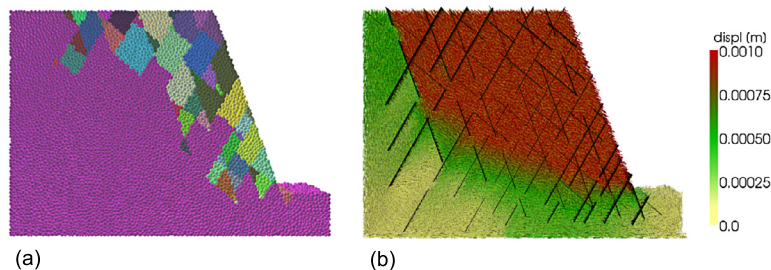
Fig. 11. (Color online.) (a) Block distribution (each color corresponds to an isolated block) and (b) post-stabilization displacement field obtained for a simulation performed on a slope with a combination of three joint sets dipping respectively 40°, 70° toward the slope face and 60° backward.

5. Conclusion

A numerical analysis of step-path failure mechanisms in jointed rock slopes is provided based upon simulations performed with an enhanced version of the discrete element method where structural defects can be simulated as pre-existing discontinuity surfaces embedded into an intact medium. The configurations studied in this paper were chosen to be relatively simple to emphasize the capability of the approach to deal with the progressive failure mechanisms developing in jointed rock slopes subjected to translational movements. Macro-fractures are simulated as a result of the coalescence of microcracks developing from the tips of the discontinuity planes in the manner of wing cracks extensions which can grow such that they eventually reach neighboring discontinuity planes and then form extended step-path failure surfaces. Both "in plane" and "out of plane" translational failures were simulated in agreement with fracture mechanics theory, confirming the critical role of tensile rupture mechanisms on the destabilization process. A sensitivity analysis performed on a slope containing a randomly distributed set of joints sharing the same preferential orientation then showed that failure develops as a result of the competition occurring between frictional mobilization on discontinuity planes and tensile fracturing of the rock bridges making up the intact part of the medium, the competition being strongly influenced by the properties of the joint network. Stress concentration in the rock bridges appears to be greatly enhanced for weaker joint mechanical properties and larger joint persistence. In the case of combined joint sets with different orientations, the method makes it possible to discriminate the respective role the different joint sets have on the overall stability and their respective prevalence toward the critical mechanisms leading to slope failure. In particular, for the tested case, the analyses showed that the most critical joint set was the one associated with toppling mechanisms, its orientation causing large and deeply seated horizontal displacements that induced irreversible damage to the slope.

Extending this work to realistic case studies, distinct configurations can be generated so as to discriminate the respective role of the geological structures present in the rock mass. Sensitivity analyses can thus be conducted in order to identify the parameters most significantly affecting the stability of a rock structure, taking into consideration the geometry of the fracture network as well as the mechanical properties of both the rock matrix and the fractures. The proposed approach appears especially suitable for the determination of critical failure surfaces as stress induced fractures basically propagate within the zones where material strength is insufficient to support the load. This is highly promising in light of the need for predicting stability of natural and artificial rock slopes for which geological data are limited or difficult to assess. Yet, care has to be taken when applying the method to real case studies given the overall uncertainty in the determination of the in situ configuration (rock mass strength, fracture distribution, joint properties, etc.). Ongoing studies are currently done to take advantage of the current efforts made in data collection methodologies and field characterization so as to more realistically capture the complexity of real rock structures.

References

[1] E. Eberhardt, D. Stead, J.S. Coggan, Numerical analysis of initiation and progressive failure in natural rock slopes – the 1991 Randa rockslide, Int. J. Rock Mech. Min. Sci. 41 (2004) 69–87.
[2] D. Stead, E. Eberhardt, J.S. Coggan, Developments in the characterization of complex rock slope deformation and failure using numerical modelling techniques, Eng. Geol. 83 (2006) 217–235.
[3] E.Z. Latjai, Shear strength of weakness planes in rock, Int. J. Rock Mech. Min. Sci. 6 (1969) 499–515.
[4] J.E. Jennings, A mathematical theory for the calculation of the stability in open cast mines, in: Planning of Open Pit Mines Proceedings, Johannesburg, South Africa, 1970, pp. 87–102.
[5] H.H. Einstein, D. Veneziano, G.H. Baecher, K.J. O'Reilly, The effect of discontinuity persistence on rock slope stability, Int. J. Rock Mech. Min. Sci. 20 (5) (1983) 227–236.
[6] M. Frayssines, D. Hantz, Failure mechanisms and triggering factors in calcareous cliffs of the Subalpine ranges (French Alps), Eng. Geol. 86 (2006) 256–270.
[7] M.A. Brideau, M. Yang, D. Stead, The role of tectonic damage and brittle rock fracture in the development of large rock slope failures, Geomorphology 103 (2009) 30–49.
[8] C. Wang, D.D. Tannant, P. Lilly, Numerical analysis of the stability of heavily jointed rock slopes using PFC2D, Int. J. Rock Mech. Min. Sci. 40 (2003) 415–424.
[9] L. Li, C.A. Tang, W. Zhu, Z. Liang, Numerical analysis of slope stability based on the gravity increase method, Comput. Geotech. 36 (7) (2009) 1246–1258.

[10] A. Vyazmensky, D. Stead, D. Elmo, A. Moss, Numerical analysis of block caving-induced instability in large open pit slopes: a finite element/discrete element approach, Rock Mech. Rock Eng. 43 (1) (2010) 21–39.

[11] P.A. Cundall, B. Damjanac, A comprehensive 3D model for rock slopes based on micromechanics, in: Slope Stability 2009, Universidad de los Andes, Santiago, Chile, 2009.

[12] L. Scholtès, F.V. Donzé, Modelling progressive failure in fractured rock masses using a 3D discrete element method, Int. J. Rock Mech. Min. Sci. 52 (2012) 18–30.

[13] K. Ma, C.A. Tang, L.C. Li, P.G. Ranjith, M. Cai, N.W. Xu, 3D modeling of stratified and irregularly jointed rock slope and its progressive failure, Arab. J. Geosci. 6 (6) (2013) 2147–2163.

[14] L. Scholtès, F.V. Donzé, A DEM model for soft and hard rocks: role of grain interlocking on strength, J. Mech. Phys. Solids 61 (2) (2012) 352–369.

[15] L. Scholtès, F.V. Donzé, M. Khanal, Scale effects on strength of geomaterials: coal case study, J. Mech. Phys. Solids 59 (5) (2011) 1131–1146.

[16] J. Kozicky, F.V. Donzé, A new open-source software developed for numerical simulations using discrete modeling methods, Comput. Methods Appl. Mech. Eng. 197 (2008) 4429–4443.

[17] J. Kozicky, F.V. Donzé, YADE-OPEN DEM: an open-source software using a discrete element method to simulate granular material, Eng. Comput. 26 (7) (2009) 786–805.

[18] V. Smilauer, E. Catalano, B. Chareyre, S. Dorofeenko, J. Duriez, A. Gladky, J. Kozicki, C. Modenese, L. Scholtès, L. Sibille, J. Stransky, K. Thoeni, Yade Documentation, The Yade Project, 1st ed., 2010, http://yade-dem.org/doc/.

[19] P.A. Cundall, O.D.L. Strack, A discrete numerical model for granular assemblies, Geotechnique 29 (1979) 47–65.

[20] D. Mas Ivars, M.E. Pierce, C. Darcel, J. Reyes-Montes, D.O. Potyondy, R.P. Young, P.A. Cundall, The synthetic rock mass approach for jointed rock mass modelling, Int. J. Rock Mech. Min. Sci. 48 (2011) 219–244.

[21] S. Bandis, A.C. Lumsden, N.R. Barton, Experimental studies of scale effects on the shear behaviour of rock joints, Int. J. Rock Mech. Min. Sci. Geomech. Abstr. 18 (1983) 1–21.

[22] H.J. Hermann, A. Hansen, S. Roux, Fracture of disordered, elastic lattice in two dimensions, Phys. Rev. B 39 (1989) 637–648.

[23] G. Liliu, J.G.M. Van Mier, 3D lattice type fracture model for concrete, Eng. Fract. Mech. 70 (7–8) (2003) 927–941.

[24] G.F. Zhao, N. Khalili, J. Fang, J. Zhao, A coupled distinct lattice spring model for rock failure under dynamic loads, Comput. Geotech. 42 (2012) 1–20.

[25] J.-P. Plassiart, N. Belheine, F.V. Donzé, A spherical discrete element model: calibration procedure and incremental response, Granul. Matter 11 (2009) 293–306.

[26] J. Sulem, H. Ouffroukh, Shear banding in drained and undrained triaxial tests on a saturated sandstone: porosity and permeability evolution, Int. J. Rock Mech. Min. Sci. 43 (2006) 292–310.

[27] J.-W. Park, J.-J. Song, Numerical simulation of a direct shear test on a rock joint using a bonded particle model, Int. J. Rock Mech. Min. Sci. 46 (2009) 1315–1328.

[28] E. Hoek, Z.T. Bieniawski, Brittle fracture propagation in rock under compression, Int. J. Fract. Mech. 1 (1965) 137–155.

[29] N. Cho, C.D. Martin, D.C. Sego, Development of a shear zone in brittle rock subjected to direct shear, Int. J. Rock Mech. Min. Sci. 45 (2008) 1335–1346.

[30] E. Hoek, E.T. Brown, Practical estimates of rock mass strength, Int. J. Rock Mech. Min. Sci. 34 (8) (1997) 1165–1186.